Hindawi
Journal of Nanomaterials
Volume 2024, Article ID 9998736, 11 pages
https://doi.org/10.1155/2024/9998736

Research Article

Differential Silica Nanoparticles Functionalized with Branched Poly(1-Vinyl-1,2,4-Triazole): Antibacterial, Antifungal, and Cytotoxic Qualities

Sedef Kaptan Usul,[1] **Hatice Büşra Lüleci**,[1] **Nurdan Sena Değirmenci**,[2] **Bengü Ergüden**,[1] **Ali Murat Soydan**,[3] **and Ayse Aslan**[1,3]

[1]*Department of Bioengineering, Gebze Technical University, Kocaeli, Türkiye*
[2]*Department of Genetic and Bioengineering, Yeditepe University, İstanbul, Türkiye*
[3]*Institute of Energy Technologies, Gebze Technical University, Kocaeli, Türkiye*

Correspondence should be addressed to Ali Murat Soydan; asoydan@gtu.edu.tr

Received 3 October 2023; Revised 23 January 2024; Accepted 9 February 2024; Published 7 March 2024

Academic Editor: Abdelwahab Omri

This research aims to improve antimicrobial materials based on functional silica nanoparticles. Three different methods were used in the study to create silica nanoparticles with other properties. The nanoparticles' morphological structures are porous, hollow, and filled with spherical forms. The surface of these nanoparticles was grafted with poly(1-vinyl-1,2,4-triazole) (PVTri). The morphological properties of nanocomposites were used for analysis. In contrast, thermal gravimetric analysis was used to characterize the thermal properties of nanocomposites (thermogravimetric analysis). The silica nanoparticles were evaluated for their *in vitro* antimicrobial activity against *Escherichia coli*, *Staphylococcus aureus*, and *Saccharomyces cerevisiae* using minimum inhibitory concentration measurement. Silica nanoparticles have different antifungal and antibacterial properties related to their structure. The cytotoxic effects of the silica nanoparticles on HaCaT cells were performed with an MTS assay. In this study, we observed that high doses of HSS and e-SiO_2 decreased cell growth, while HSS and e-SiO_2 composite with PVTri increased cell proliferation.

1. Introduction

Silica particles are highly interesting among various inorganic nanoparticles due to their excellent chemical properties. Silica nanoparticles are compatible with other materials thanks to their stability, thermal properties, low density and toxicity, and excellent biocompatibility. They can also be easily functionalized to bind other active materials chemically [1, 2].

Porous silica nanoparticles (MSN) are used in biomedical, pharmaceutical, and biochemistry applications due to their large surface area, stability, and biocompatibility [3, 4]. In addition, thanks to the siloxane bonds (Si—O—Si) in the structure of MSNs, they are mechanically stable and resistant to microbial attacks. Synthesis of MSNs is convenient and low-cost [5, 6]. When silica is broken down metabolically, it produces silicic acid byproducts. Silicic acid acts as a biostimulant system, reducing toxicity, and disease resistance [7].

Silica nanoparticles with the desired particle shape, size porosity, and crystallinity can be produced by being designed appropriately. The sol–gel and template-assisted synthesis processes are widely used to create single-pore silica (HSS). Changes in pH or temperature can alter the shape of nanoparticles. HSSs-containing monodisperse phenyl groups are made without structure by dissolving in organic solvents [8, 9].

Modifying the surface of silica nanoparticles with epoxide structures improves the particle's properties. As with conventional organic polymer modifications, epoxide-modified nanocomposites are of awesome impression by the reason of their excellent adhesion, high corrosion resistance, thermal stability, and low impurities. Therefore, such hybrid systems allow the use of many industrial epoxy formulations today [10, 11]. In addition to these unique properties, it is known

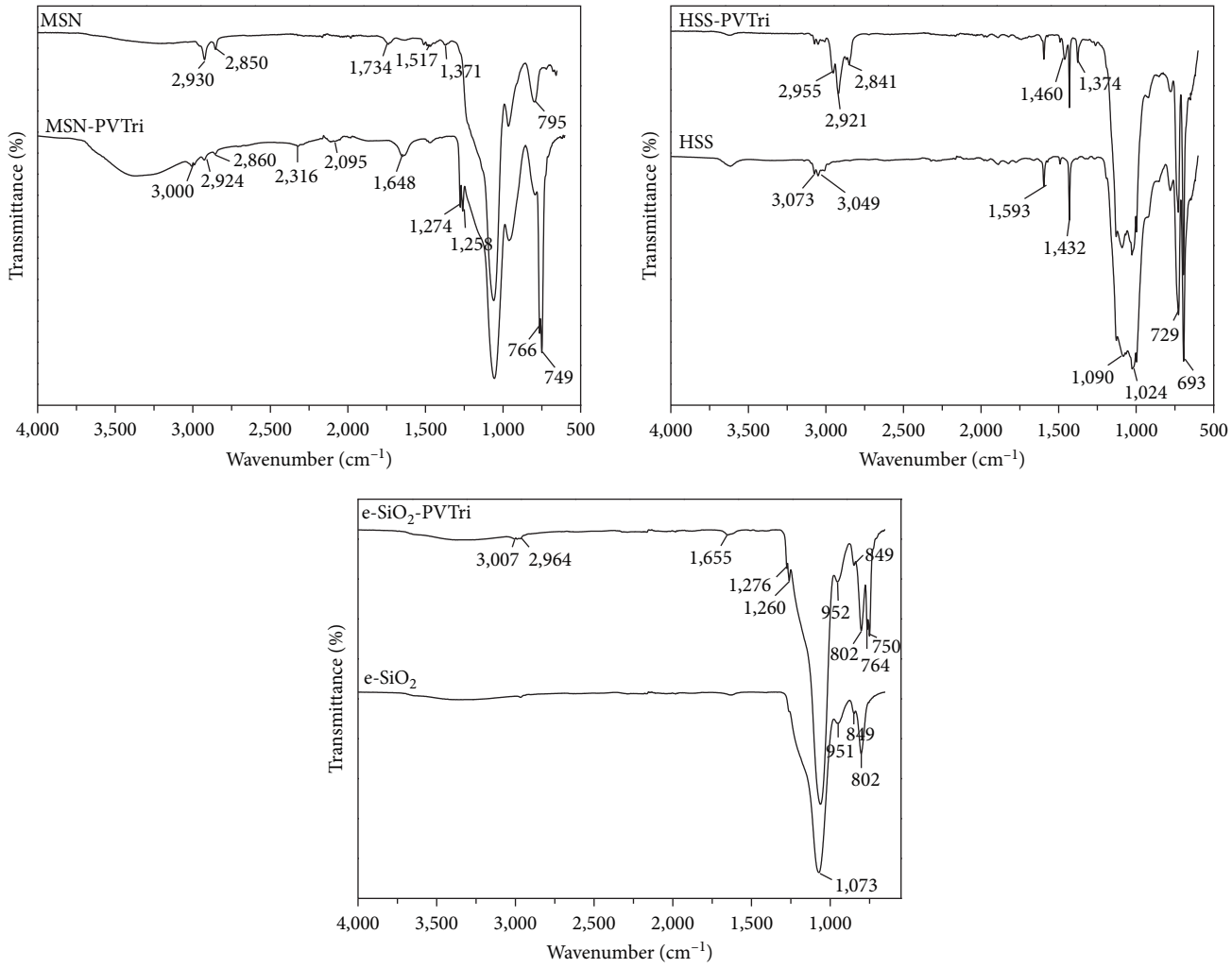

Figure 1: FTIR spectrums of MSN-PVTri, HSS-PVTri, and e-SiO_2-PVTri.

that when nanoparticles and epoxides come together, they can fill the micron cracks and defects in the structure, improving its chemical structure. In addition, the epoxy rings formed on silica nanoparticles' surfaces (e-SiO_2) allow easy modification of the material [11].

Azole groups demonstrate good antimicrobial activity against bacterial strains [12, 13]. Synthesized silica nanoparticles can be used in various biological applications because of their antimicrobial properties, thanks to azole groups [14]. All antimicrobial azoles work primarily by inhibiting the cytochrome P450 enzyme 14-alpha-demethylase. The azole group's free nitrogen atom binding to the prosthetic group's iron in the enzyme's active site causes inhibition. The unique properties of these azole-containing structures allow their use in biomedical applications, chemistry, and food industries [15, 16]. PVTri is the most exciting monomer besides its antimicrobial effect. It also has several properties: thermal stability and endurance to attacker environments, elaborate formation, and quantization. Furthermore, it has high biocompatibility and a controllable molecular weight [17–19]. In this study, silica nanoparticles' design, synthesis, and antibacterial and antifungal activities involving azole groups have been comprehensively researched, and it will become one of the maximumly active highlights in recent years. Three different silica nanoparticles were synthesized and characterized. Their antifungal and antibacterial properties were detected using different strains, and it can be said that they have antimicrobial effects based on their structural properties.

2. Materials and Methods

2.1. Materials. 1-Vinyl-1,2,4-triazole (VTri, >97%), toluene (>99%), trimethoxymethylsilane (PTMS, 95%), tetraethyl orthosilicate (TEOS, 98%), dimethyl sulfoxide (DMSO, >99), hexadecyltrimethylammonium bromide (CTAB), dimethyldodecylethylammonium bromide (EDMAB, ≥98%), camforquinone (Cq) was provided from Sigma Aldrich. For yeast and D-Glucose, yeast extract powder, peptone, and agar powder were provided for yeast and bacterial strains. Yeast and bacterial strains were obtained from the Mycology and Microbiology Laboratory, Gebze Technical University, Kocaeli, Turkey.

2.2. Synthesis and Modification of Porous Silica Nanoparticles. MSNs were created through a sol–gel reaction of TEOS and

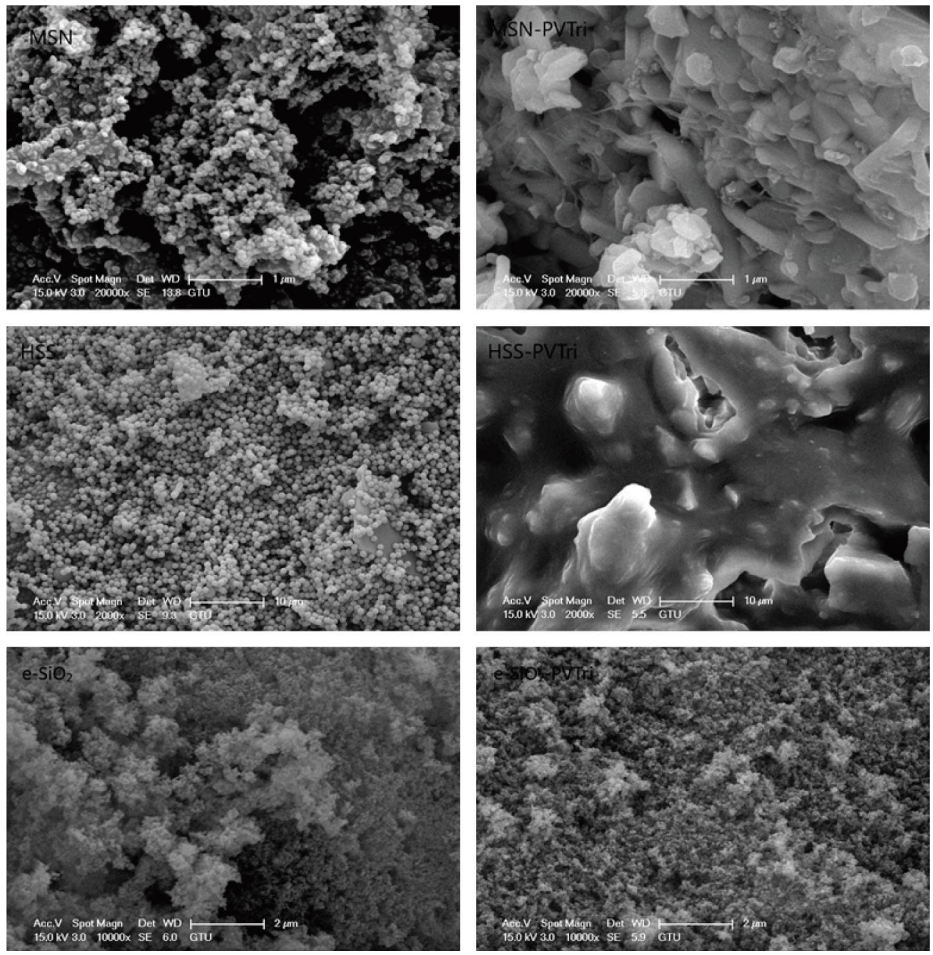

FIGURE 2: SEM images MSN, MSN-PVTri, HSS, HSS-PVTri, e-SiO_2, and e-SiO_2-PVTri.

the cationic surfactant CTAB [20, 21]. Antimicrobial nanocomposite was synthesized by photopolymerization reaction of VTri monomer on the surface of MSN nanoparticles. Using Cq, the reaction was incubated for 2 hr under a nitrogen atmosphere and temperature of 80°C. MSN-PVTri nanocomposite was washed with a toluene mixture several times after precipitation with THF [18, 22].

2.3. Synthesis and Modification of Hollow Silica Nanoparticles. This study used the two-stage sol–gel method to create single-pore silica particles. Under acidic conditions, PTMS was hydrolyzed solution of 0.66×10^{-2} M HNO_3 was placed in a water bath. The resolution was treated with PTMS, and the mixture solution was stirred. In the second step, NH_4OH solution was added to the solution for condensation. The transparent reaction, which turned milky, was continuously stirred for 1 hr [9]. The HSS-PVTri nanocomposite was carried out in the same way as the synthesis of the MSN-PVTri nanocomposite [23].

2.4. Modification of Epoxy Silica Nanoparticles. Epoxy silica nanoparticles (e-SiO_2) were obtained from the brand Sky Spring Nanomaterials (Houston, USA) and are 10–20 nm in size. e-SiO_2-PVTri nanocomposite was synthesized by photo polymerization by dispersing e-SiO_2 and VTri monomers in toluene (80°C, 2 hr) [24].

2.5. Characterization of Prepared Nanocomposites. Fourier-transform infrared spectroscopy (FTIR) and X-ray diffraction method (XRD) were put to use to search for the successful surface polymerization of VTri with the synthesis of MSN, HSS, and e-SiO_2. Based on the relevant functional group absorption, the FTIR spectra recorded for MSN, MSN-PVTri, HSS, HSS-PVTri, e-SiO_2, and e-SiO_2-PVTri 4,000–400 cm^{-1} were compared and evaluated. Scanning electron microscopy (SEM) uses the porous structures and modification of MSN, MSN-PVTri, HSS, HSS-PVTri, e-SiO_2, and e-SiO_2-PVTri particles. Atomic contents of nanocomposites were investigated by energy-dispersive spectroscopy (EDS). Thermogravimetric analysis (TGA) was used to evaluate and quantify the modification of nanoparticles and nanocomposites.

2.6. Minimum Inhibitory Concentration (MIC) Measurement. MIC measurement was used to evaluate the antifungal and antimicrobial activity of the synthesized silica nanoparticles. MIC measurements were performed for *Saccharomyces cerevisiae* (MATa ura3-52 lys2-801_amber ade2-101_ochre trp1-Δ63 his3-Δ200 leu2-Δ1 [24]) yeast cells like the study Konuk

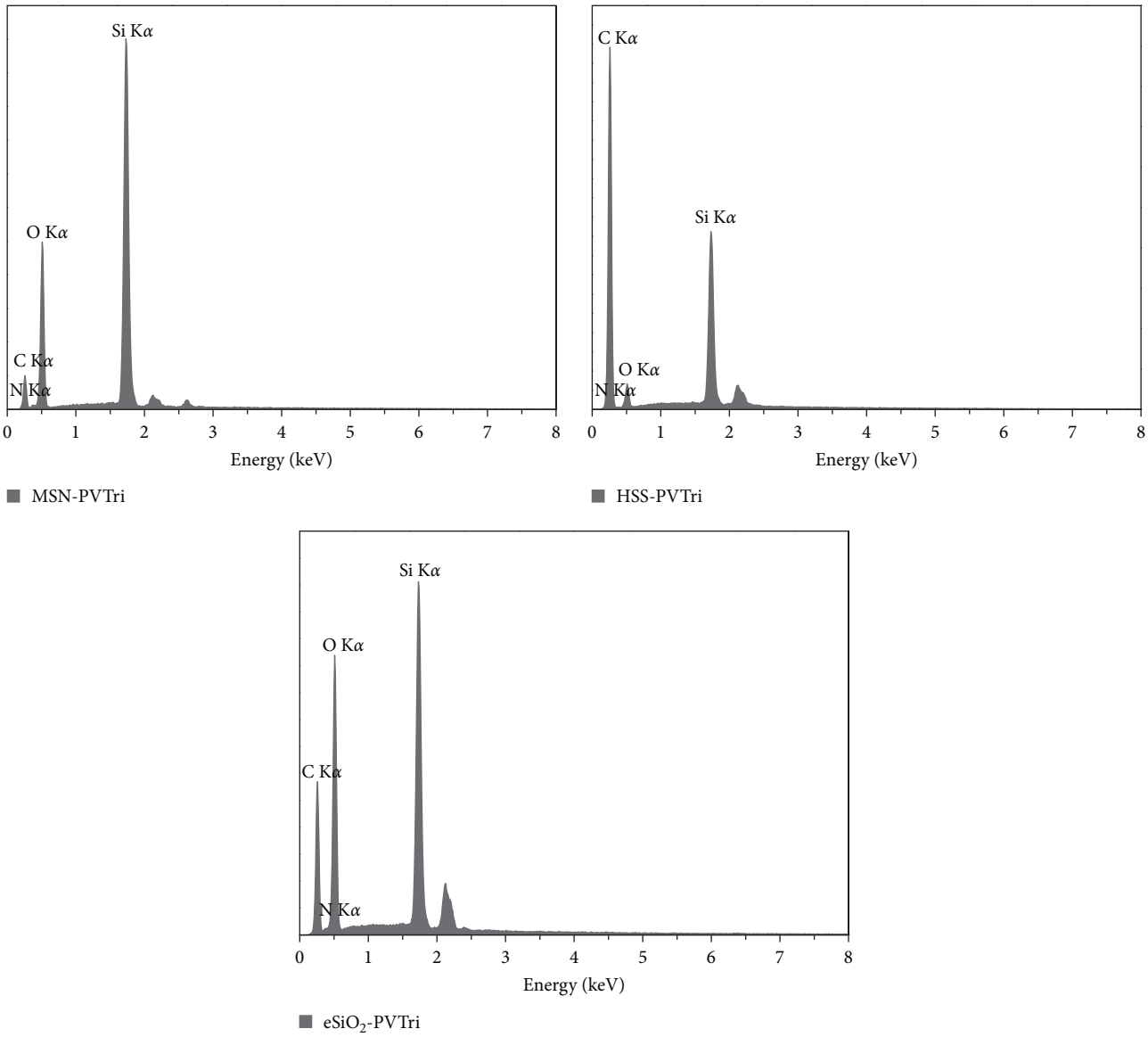

Figure 3: EDS graphs of MSN-PVTri, HSS-PVTri, and e-SiO_2-PVTri.

Table 1: The mass atomic percentages of functional nanoparticles.

Element (wt%)	C	N	O	Si
MSN	21.42	—	38.42	38.18
MSN-PVTri	23.33	4.18	41.08	31.41
HSS	50.13	—	14.03	35.84
HSS-PVTri	79.17	1.89	8.44	10.51
e-SiO_2	9.46	—	46.95	41.53
e-SiO_2-PVTri	37.22	3.19	43.42	16.17

and Ergüden [25]; for Gram-negative *Escherichia coli* (ATCC® PTA-5976TM) and Gram-positive *Staphylococcus aureus* (ATCC® 25923™) bacteria cells like the study by Ergüden [26]. Different concentrations of 1, 5, and 10 mg/mL of silica nanoparticles scattered in DMSO were insetted to the plate to determine inhibition concentrations. The lowest nanocomposite concentration with no visible growth of yeast or bacterial cells was accepted as the MIC value for each silica nanoparticle. Sampling was prepared in triplicate for each concentration, and the experiment was repeated three times.

2.7. Cell Culture. Human keratinocyte cell line HaCaT (CLS 300493, DKFZ, Heidelberg, Germany) was put to use for this study. HaCat cells (5,000 cells/well) were cultured in DMEM

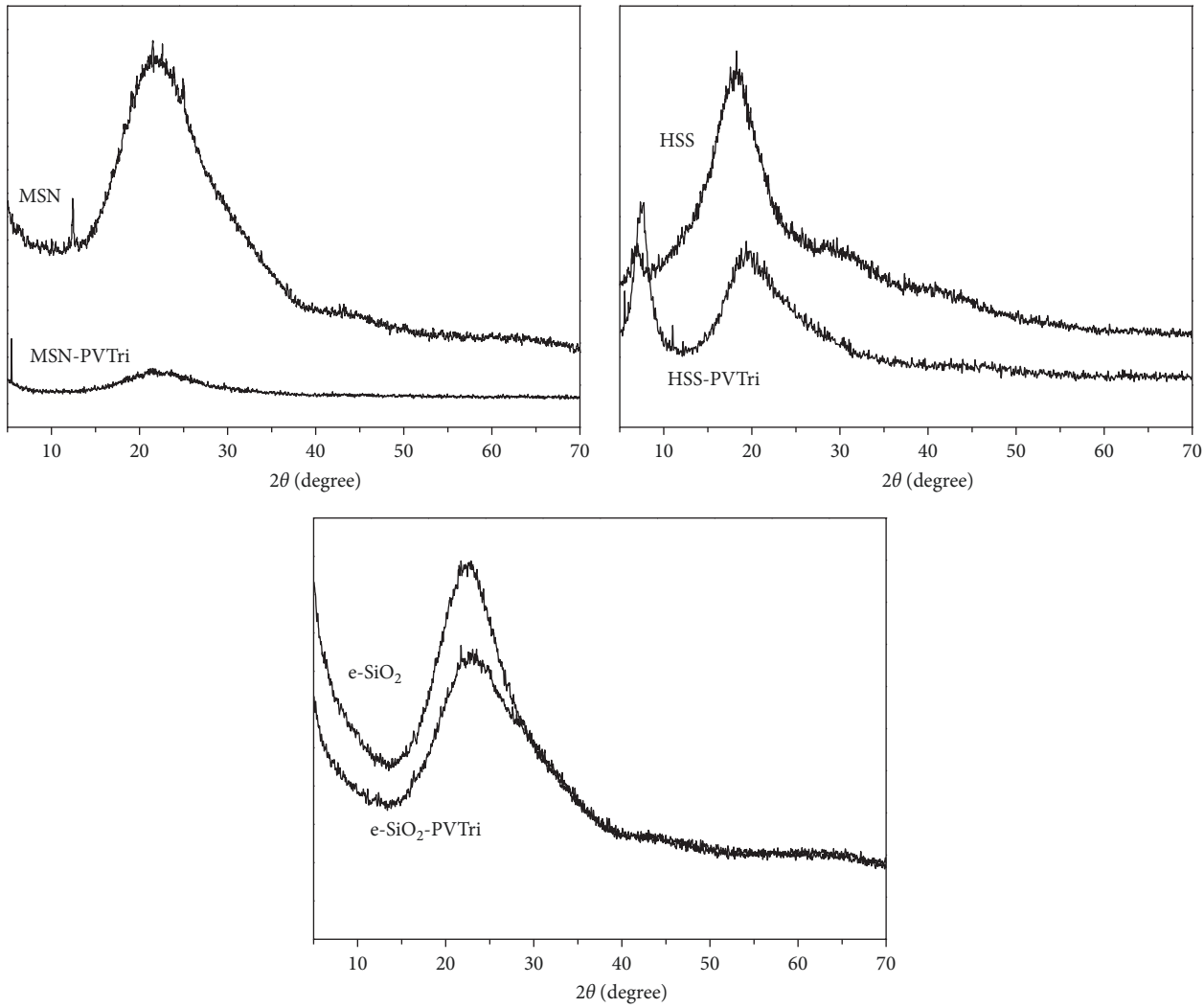

FIGURE 4: XRD graphs of MSN-PVTri, HSS-PVTri, and e-SiO_2-PVTri.

(Gibco BE12-702F, Thermo Fisher Scientific, USA) supplemented with 10% FBS and 100 units/mL of penicillin, 100 μg/mL of streptomycin and amphotericin (1% PSA, Invitrogen, Gibco, UK). (PSA, Invitrogen, Gibco, UK). The cells were cultured in the humidified incubator at 37°C, 95% air, and 5% CO_2 conditions [27].

2.8. Cell Cytotoxicity Assay. HACAT cells were seeded onto 96-well plates (TPP, Switzerland) at a density of 5,000 cells/well. The various concentrations of the silica nanoparticles were dissolved in DMEM high glucose media. After 24 hr, the cells were processed with stated concentrations of silica nanoparticles (1, 0.5, and 0.25 mg/mL) for 24, 48, and 72 hr. Cell viability was measured by the MTS reagent (G3582, CellTiter96 Aqueous One Solution; Promega, Southampton, UK) according to the manufacturer's instructions. Absorbance at 490 nm was detected using an ELISA plate reader (Biotek, Winooski, VT). The percentage of cell viability was calculated according to the control cells (nontreated for silica nanoparticles) [28]. All study was performed in triplicate.

3. Results

3.1. FTIR Analysis. The polymerization of the samples analyzed was used using FTIR spectroscopy. The infrared spectra of MSN and MSN-PVTri nanoparticles are shown in Figure 1. At 1,064 and 800 cm^{-1}, it indicates asymmetric and symmetric stretching vibrations of Si—O—Si bonds. The stretching vibrations of the Si—OH and O—H groups are assigned to the peaks at 977 and 3,300 cm^{-1}, respectively. Peaks at 2,900 and 3,300 cm^{-1} are caused by stretching vibrations of the C—H and OH bonds, respectively, and are most likely caused by residual CTAB that was not removed by acid etching. By polymerizing VTri to the surface, triazole rings form several moderately strong peaks in the 1,430–1,650 cm^{-1} range due to ring stretch (C—N, C═N) vibrations. The peak at 1,274 cm^{-1} is due to stretching the N—N ring. The broad peak centered at 3,430 cm^{-1} is assigned to the O—H vibration of molecular water interacting with pristine PVTri [21, 29]. The HSS spectra show a strong absorption peak of the Si—O—Si asymmetric stretch at 1,090 cm^{-1}. The peaks at 782 cm^{-1} can be attributed to the symmetrical

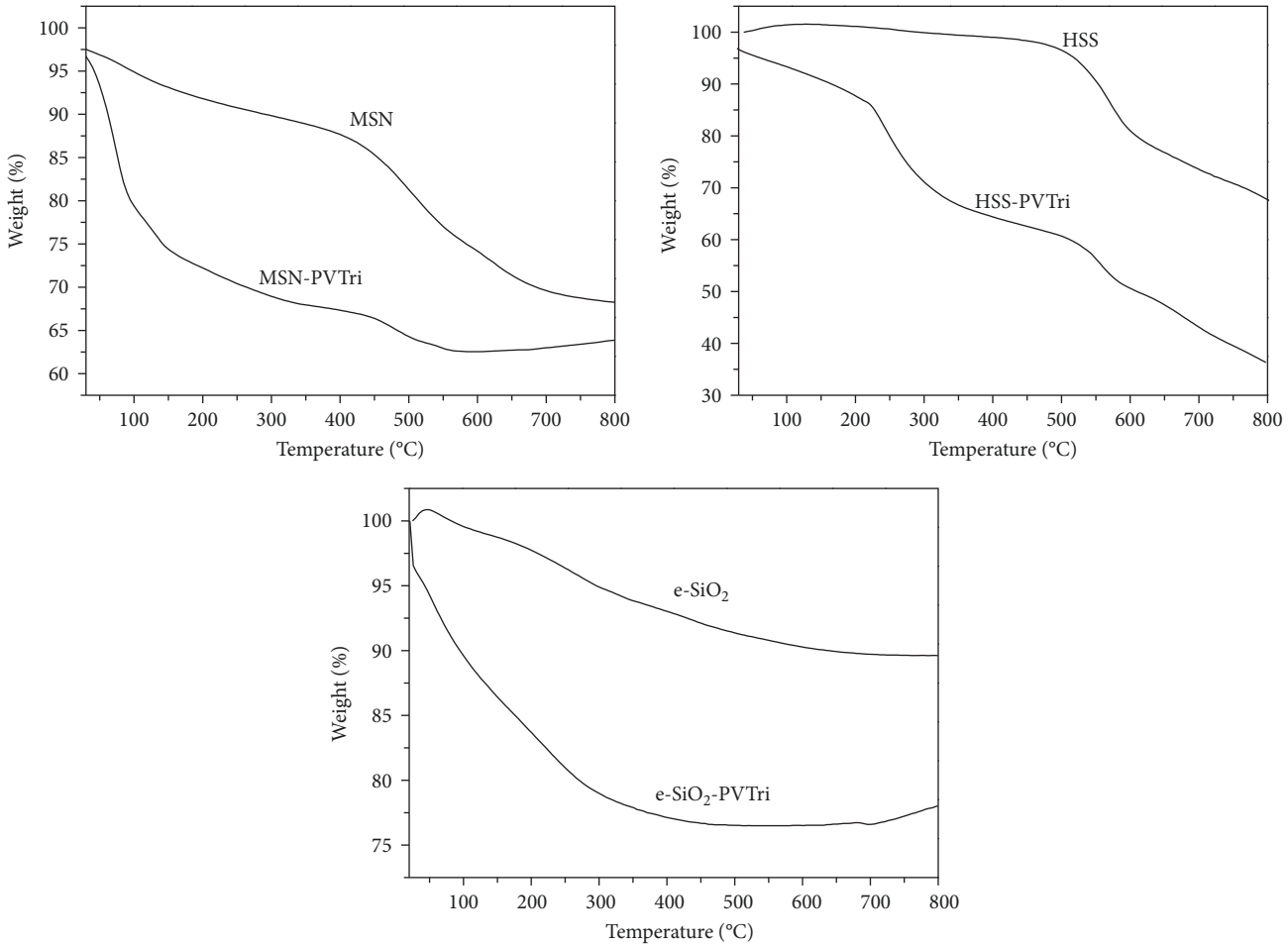

Figure 5: TGA graphs of MSN-PVTri, HSS-PVTri, and e-SiO_2-PVTri.

Table 2: MIC values (mg/mL) for *S. cerevisiae*, *E. coli*, and *S. aureus*.

Nanocomposites	*S. cerevisiae*	*E. coli*	*S. aureus*
MSN-PVTri	0–1	0–1	5–10
HSS-PVTri	>10	5–10	>10
e-SiO_2-PVTri	>10	1–5	>10

stretching vibration of Si—O, while the peak at 936 cm^{-1} could be attributed to the bending vibration of Si—OH. At around 3,600 cm^{-1}, a weak but distinct Si—OH stretching vibration can be seen. The peak at 3,073 cm^{-1} is attributed to the asymmetric stretching vibration of aromatic phenyl C–H groups bound to HSS. By polymerizing VTri on the surface, triazole rings form several moderately strong peaks in the 1,430–1,650 cm^{-1} range due to ring stretch (C—N, C═N) vibrations [22]. The wide band e-SiO_2 of the FTIR figure at 1,073 cm^{-1} originates from the epoxy ring. After the surface was modified with VTri, a peak from the triazole structure was formed at 1,655 cm^{-1}. In addition, the peaks at the mountains and 750 cm^{-1} are specific to VTri. The peaks observed at 782 cm^{-1} can be assigned to the symmetrical stretching vibration of Si—O bond [30, 31].

3.2. SEM–EDS Analysis. SEM examined nanoparticles and nanocomposites of the surface morphologies. Figure 2 depicts the structural change caused by grafting on the MSN surface. When comparing natural and polymer-modified particles, a clear difference can be seen. The polymer covers the particle surface, but growth occurs as well in forming some irregularly shaped particles. Figure 2 illustrates the polymerization reaction of VTri azole monomers occurring on the surface of HSS nanoparticles. Moreover, by coating the surface of HSS nanoparticles with a VTri monomer, the spherical particles became trapped in the bulk polymer. e-SiO_2 of the SEM image revealed a high degree of accumulation due to the nanostructure. However, individual nanoparticles were observed in the 40–50 nm range, agreeing with the crystallite size informed by the X-ray line profile insertion. There was no significant increase in size with the modification of the surface. Figure 3 and Table 1 represent the outcomes of the EDS analysis of the nanocomposites. As seen in the EDS shapes of the nanocomposites, the presence of C, O, N, and Si atoms in their contents

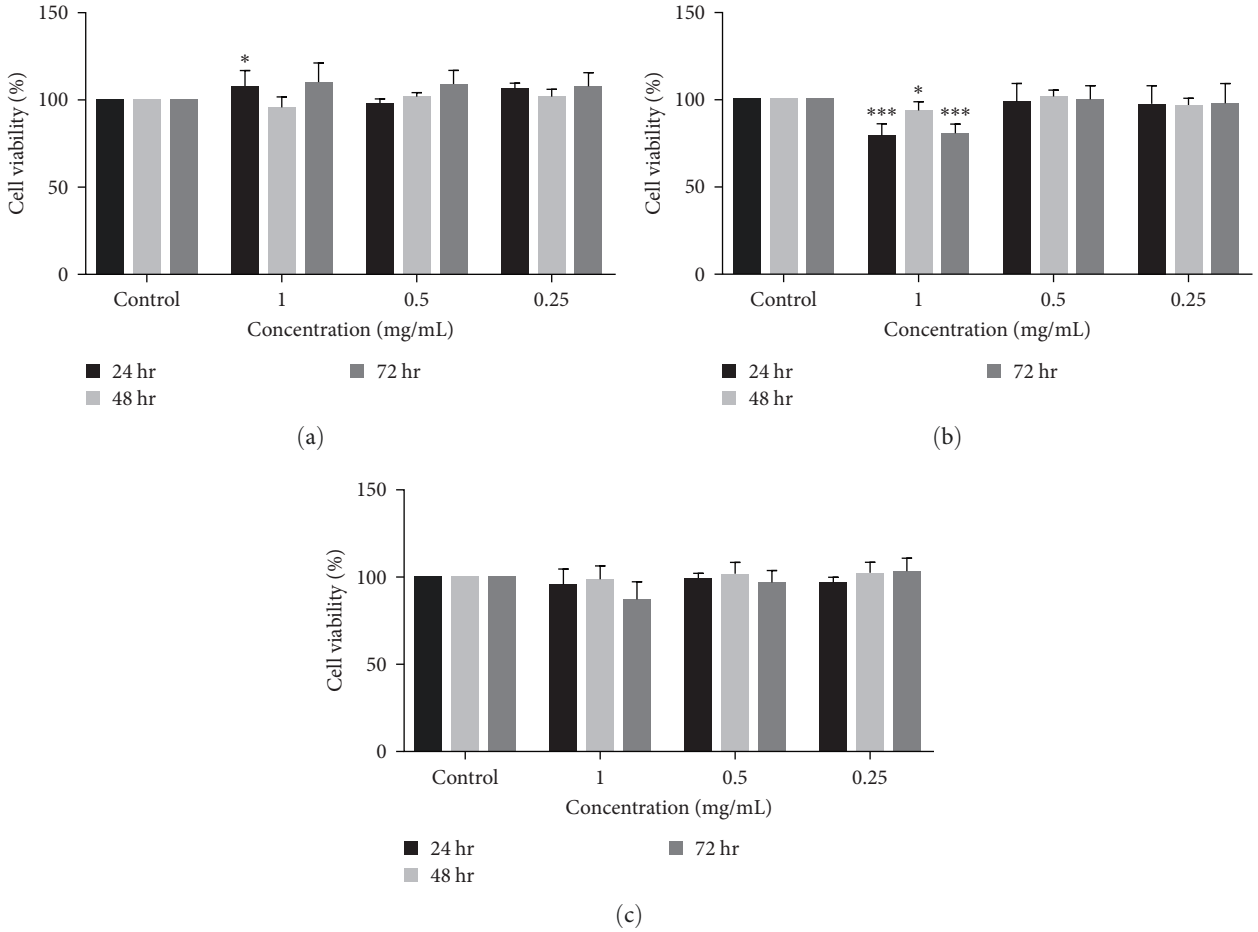

Figure 6: Cell proliferation assay on HaCaT keratinocyte cell line: (a) different concentrations (1, 0.5, and 0.25 mg) of PVTri; (b) different concentrations (1, 0.5, and 0.25 mg) of e-SiO_2; (c) different concentrations (1, 0.5, and 0.25 mg) of HSS were treated HaCaT cells at 24, 48, and 72 hr by using MTS assay and absorbance was measured at 490 nm by using a microplate reader. Data shows average of experiments repeat three times ± SD ($^{***}p \leq 0.001$, $^{*}p \leq 0.05$).

has been confirmed. MSN-PVTri (31.41%) nanocomposite has the highest percentage of Si atoms by mass, while the percentage of C atoms by mass is the highest in HSS-PVTri (79.17%) nanocomposite. As can be seen from the EDS results, MSN-PVTri, the nanocomposite with the highest nitrogen content, is the material that contains the most azole groups on its surface.

3.3. XRD Analysis. XRD did a phase investigation of MSN with MSN-PVTri, HSS with HSS-PVTri, and e-SiO_2 with e-SiO_2-PVTri. The diffraction pattern is presented in Figure 4. The MSN nanoparticle peaks around 2θ at 21.6°; it is seen in amorphous form. The decrease in density at 21.6° with the surface modification proves that the change has occurred. The HSS nanoparticle has a peak visible at 18.2° around 2θ, and it is seen that it is in amorphous form. The decrease in density at 19.4° with the surface modification proves that the change has occurred. And also, e-SiO_2 and e-SiO_2-PVTri are amorphous forms at 22.5° around 2θ.

3.4. TGA. Weight loss graphs of TGA prove the existence of polymer grown from nanoparticles. Thermally stable compounds that remain in the residue (polymer-bound silica) and degradable polymer structures and initiators contribute to weight loss in the coated particles. The thermal stability of the PVTri polymer is 300−350°C [32]. The thermal degradation curves show that the thermal stability of the MSN-PVTri nanocomposite, formed after the vinyltriazole monomer is grown on the surface of the MSN nanoparticle, has increased to 400°C. After VTri polymerization on the surface of the HSS nanoparticle, TGA, a total weight loss of 40% is seen in Figure 5. Moreover, it was sighted that the thermal stability of e-SiO_2 nanoparticles increased after polymerization and preserved its structure by 85% above 800°C.

3.5. MIC. The study tested the antifungal and antibacterial properties of nanocomposites whose surfaces were modified with vinyltriazole with the MIC measurement. The MIC values of MSN-PVTri nanoparticle are 0–1 mg/mL for *S. cerevisiae* and *E. coli*, while for *S. aureus* bacterium, it is 5–10 mg/mL. The MIC values of HSS-PVtri and e-SiO_2-PVTri nanoparticles have shown different values for the same yeast and bacteria (Table 2).

3.6. Effect of Silica Nanoparticles on HaCaT Keratinocytes. The cytotoxic effects of various silica nanoparticles were

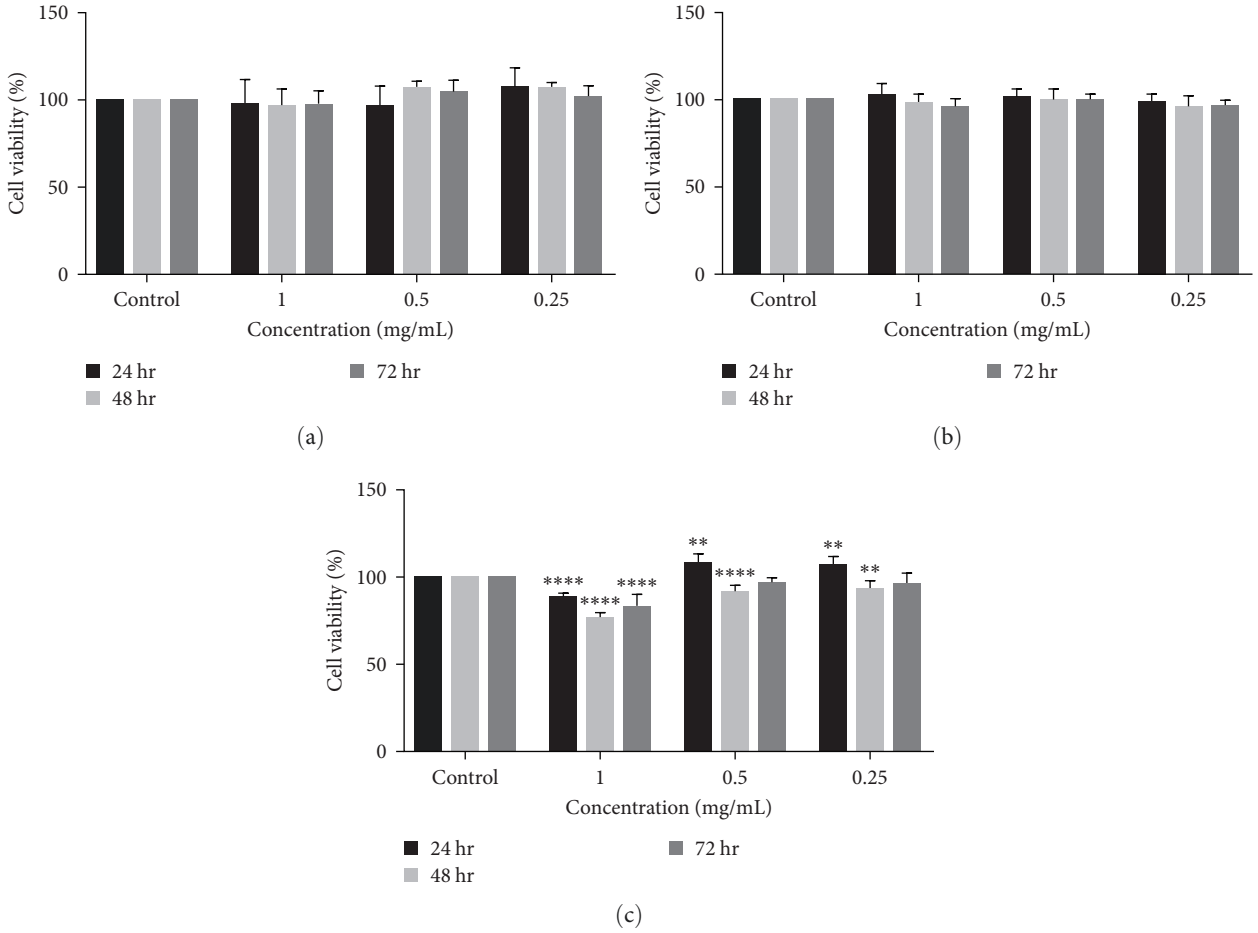

Figure 7: Cell proliferation assay on HaCaT keratinocyte cell line: (a) different concentrations (1, 0.5, and 0.25 mg) of e-SiO_2-PVTri; (b) different concentrations (1, 0.5, and 0.25 mg) of HSS—PVTri; (c) different concentrations (1, 0.5, and 0.25 mg) of MSN-PVTri were treated HaCaT cells at 24, 48, and 72 hr by using MTS assay and absorbance was measured at 490 nm by using a microplate reader. Data shows average of experiments repeat three times ± SD ($^{****}p \leq 0.0001$, $^{**}p \leq 0.01$).

determined and compared with the control group (non-treated for silica nanoparticles) on HaCaT cells. HaCat cells were treated with different concentrations of e-SiO_2, HSS, PVTri, e-SiO_2-PVTri, HSS-PVTri, and MSN-PVTri ranging from 1 to 0.25 mg for the 24, 48, and 72 hr (Figures 6 and 7). Based on the MTS results, it was shown that all PVTris, except for e-SiO_2 1 mg/mL, did not exhibit cytotoxic effects on HaCaT cells.

4. Discussion

4.1. Characterization of Functional Nanocomposites. The FTIR graph in Figure 1 demonstrates that the strain on the C—N and C=N bonds at 1,430–1,650 cm^{-1} of the VTri monomer indicates the functionalization of silica nanoparticles. This is further supported by the peak at 1,274 cm^{-1} corresponding to the N—N bond. The peaks corresponding to azolic groups, resulting from the grafting of VTri monomers onto the surface of nanoparticles, confer antimicrobial properties to the nanocomposites. Therefore, the occurrence of peaks within the range of 1,430–1,650 cm^{-1} and 1,274 cm^{-1} in the FTIR spectra of the three nanocomposites is crucial and signifies the presence of these functional groups essential for antimicrobial activity [33, 34]. SEM images in Figure 2 clearly indicate the presence of polymerization on the surfaces of MSN, HSS, and e-SiO_2 nanoparticles. The EDS graphs for functionalized nanoparticles not only show the distribution of atoms but also specify the mass percentages of C, N, O, and Si atoms in Table 1. The antimicrobial properties of nanocomposite structures remain unaffected by the presence of C, O, and Si atoms. The enhancement in antimicrobial activity is attributed to the azolic structures within the VTri configuration, with an increase in the N atom content contributing to the heightened antimicrobial activity of the nanocomposite structure. The XRD pattern indicates the polymerization on the surfaces of the nanoparticles. The TGA graphs of the materials demonstrate that the functionalized MSN and e-SiO_2 nanoparticles are more durable than HSS upon thermal degradation.

4.2. MIC. All three nanoparticles are more impressive against Gram-negative bacteria than Gram-positive ones and yeast strains. MSN-PVTri has smaller MIC values (0–1 mg/mL for *S. cerevisiae* and *E. coli* and 5–10 mg/mL for *S. aureus*) because of its higher antifungal and antibacterial activities. The larger porous surface area of the MSN nanoparticle

compared to HSS and e-SiO_2 provides more vinyltriazole monomer binding to the surface and high antimicrobial activity. The HSS and e-SiO_2 nanoparticles have similar effects on the *S. cerevisiae* and *S. aureus* cells (MIC: >10 mg/mL). On the other hand, e-SiO_2 is more effective (MIC: 1–5 mg/mL) compared to HSS nanoparticles (MIC: 5–10 mg/mL) in the *E. coli* cells. The e-SiO_2 nanoparticle has more vinyltriazole monomer binding side on its surface because of the epoxy ring compared to the HSS nanoparticle. For this reason, it is more effective than HSS nanoparticles on Gram-negative bacteria.

4.3. Effect of Silica Nanoparticles on HaCaT Keratinocytes. Primary keratinocytes require supplementary growth factors for their survival in a laboratory environment and exhibit rapid cell death, posing challenges for research activities. Hacat human keratocytes that have been immortalized can be cultivated in standard media and have an extended lifespan in culture. Furthermore, Hacat cells exhibit all the functional characteristics of typical keratinocytes when cultivated in a controlled environment [35]. In this study, we used HaCaT cells to investigate the cytotoxic effects of PVTri. Our data have shown that all concentrations of PVTri increased cell proliferation when applied alone for 24, 48, and 72 hr on HaCaT cells. Although 1 mg concentration of e-SiO_2 treatment significantly decreased the cell proliferation for 24 and 72 hr on HaCat cells, all the concentrations of e-SiO_2-PVTri (1, 0.5, and 0.25 mg/mL) increased the cell proliferation for 24, 48, and 72 hr on HaCat cells. HaCaT cells were treated at various concentrations of HSS nanoparticles (1, 0.5, and 0.25 mg/mL). Our results indicated that the 1 mg concentration of HSS—PVTri nanocomposite more increased cell proliferation than the treatment of HSS (1 mg) nanoparticle on HaCaT cells for 24, 48, and 72 hr. HaCaT cells were also treated with MSN-PVTri (1, 0.5, and 0.25 mg/mL) nanoparticles for 24, 48, and 72 hr. According to these results, unlike the other two nanocomposites, all concentrations of MSN-PVTri treatment significantly reduced cell growth on HaCaT cells. In this study, we demonstrated that all nanocomposites that contain with PVTri increased the cell proliferation on HaCaT keratinocyte cells, except MSN nanoparticles.

5. Conclusion

This study investigated the characterization, antimicrobial, and cytotoxic effects of synthesized MSN-PVTri, HSS-PVTri, and e-SiO_2-PVTri nanocomposites.

(1) The modification of nanocomposites has been demonstrated by FTIR and SEM–EDS analysis.
(2) After conversion, the thermal stability of MSN-PVTri and e-SiO_2-PVTri nanocomposites increased, while HSS-PVTri nanocomposite decreased.
(3) As a result of XRD analysis, the peak value after modification of nanoparticles in amorphous structure decreased in all nanocomposites.
(4) MSN-PVTri nanocomposite interacts more with vinyltriazole than HSS-PVTri and e-SiO_2-PVTri nanocomposite due to its higher surface porosity and bonding groups.
(5) MIC measurement showed that MSN-PVTri has more antimicrobial activity than HSS-PVTri and e-SiO_2-PVTri because of its sizeable porous surface. Moreover, e-SiO_2-PVTri has more antibacterial activity for Gram-negative bacteria than HSS-PVTri because of its epoxy ring on its surface.
(6) Cytotoxic analysis has evaluated that when PVTri binds to HSS and e-SiO_2 nanoparticles, it increases cell growth in HaCaT cells.

In summary, the envisioned new nanocomposites demonstrate outstanding potential for biological applications owing to their notable antimicrobial and antitoxic properties. Future research endeavors may focus on enhancing the monomer binding rate and polymerization rates on the surface of MSN-PVTri. Mechanical and animal experiments, along with surface coating, could further elucidate the suitability of these nanocomposites for diverse applications, including the paint industry.

Data Availability

The data used to support the findings of this study have been deposited in the "Research Square" repository (https://doi.org/10.21203/rs.3.rs.-3095931/v1).

Additional Points

Highlights. (i) Functional nanoparticles are used in a variety of bioengineering applications. (ii) Vinyltriazole has unique antimicrobial properties. (iii) The amount of vinyltriazole monomer attached to the surface of the silica material affects the antimicrobial property.

Disclosure

"A preprint has previously been published (Usul, S. K. et al., 2023)." The study was conducted at Gebze Technical University as part of the authors' employment.

Conflicts of Interest

The authors declare that there are no conflicts of interest regarding the publication of this paper.

Authors' Contributions

Sedef Kaptan Usul has contributed to the term, conceptualization ideas, methodology development or design of methodology, validation verification, investigation, resources, writing—review and editing, visualization, and project administration. Hatice Büşra Lüleci has contributed to the writing—review and editing, visualization, methodology development, or design of methodology. Nurdan Sena Değirmenci has contributed to the writing—review and editing, visualization, methodology development, or design of methodology. Bengü Ergüden has

contributed to the writing—review and editing, visualization, methodology development, or design of methodology. Ali Murat Soydan has contributed to the resources, writing—review and editing, and financial support. Ayşe Aslan Canpolat has contributed to the term, conceptualization ideas, methodology development or design of methodology, investigation, resources, writing—review and editing, visualization, and financial support.

References

[1] S. K. Usul, H. B. Lüleci, N. S. Değirmenci, B. Ergüden, and A. Aslan, *Differential silica nanoparticles functionalized with branched poly(1-Vinyl-1,2,4-triazole): antibacterial, antifungal, and cytotoxic qualities*, pp. 1–18, 2023.

[2] I. Zarafu, A. A. J. Al Taweel, C. Limban et al., "Aminopropyl-silica functionalized with halogen-reactive compounds for antimicrobial applications," *Materials Chemistry and Physics*, vol. 241, Article ID 122353, 2020.

[3] W. Lu, M. Chen, M. Cheng et al., "Development of antioxidant and antimicrobial bioactive films based on Oregano essential oil/mesoporous nano-silica/sodium alginate," *Food Packaging and Shelf Life*, vol. 29, Article ID 100691, 2021.

[4] S. Ribes, M. Ruiz-Rico, É. Pérez-Esteve et al., "Eugenol and thymol immobilised on mesoporous silica-based material as an innovative antifungal system: application in strawberry jam," *Food Control*, vol. 81, pp. 181–188, 2017.

[5] K. M. Fuentes, D. Onna, T. Rioual et al., "Copper upcycling by hierarchical porous silica spheres functionalized with branched polyethylenimine: antimicrobial and catalytic applications," *Microporous and Mesoporous Materials*, vol. 327, Article ID 111391, 2021.

[6] J. Sun, Y. Fan, P. Zhang et al., "Self-enriched mesoporous silica nanoparticle composite membrane with remarkable photodynamic antimicrobial performances," *Journal of Colloid and Interface Science*, vol. 559, pp. 197–205, 2020.

[7] M. J. Ndolomingo, N. Bingwa, and R. Meijboom, "Review of supported metal nanoparticles: synthesis methodologies, advantages and application as catalysts," *Journal of Materials Science*, vol. 55, no. 15, pp. 6195–6241, 2020.

[8] M. Sattary, J. Amini, and R. Hallaj, "Antifungal activity of the lemongrass and clove oil encapsulated in mesoporous silica nanoparticles against wheat's take-all disease," *Pesticide Biochemistry and Physiology*, vol. 170, Article ID 104696, 2020.

[9] A. Derbalah, M. Shenashen, A. Hamza, A. Mohamed, and S. El Safty, "Antifungal activity of fabricated mesoporous silica nanoparticles against early blight of tomato," *Egyptian Journal of Basic and Applied Sciences*, vol. 5, no. 2, pp. 145–150, 2019.

[10] A. Aslan, S. Elanthikkal, and A. Bozkurt, "Chitosan/hollow silica sphere nanocomposites for wound healing application," *Journal of Materials Research*, vol. 34, no. 2, pp. 231–239, 2019.

[11] S. Sprenger, "Epoxy resins modified with elastomers and surface-modified silica nanoparticles," *Polymer*, vol. 54, no. 18, pp. 4790–4797, 2013.

[12] P. Rosso and L. Ye, "Epoxy/silica nanocomposites: nanoparticle-induced cure kinetics and microstructure," *Macromolecular Rapid Communications*, vol. 28, no. 1, pp. 121–126, 2007.

[13] F. Samrin, A. Sharma, I. A. Khan, and S. Puri, "Synthesis and antibacterial activity of new diaryldiamines," *Journal of Heterocyclic Chemistry*, vol. 49, no. 6, pp. 1391–1397, 2012.

[14] X.-M. Peng, G.-X. Cai, and C.-H. Zhou, "Recent developments in azole compounds as antibacterial and antifungal agents," *Current Topics in Medicinal Chemistry*, vol. 13, no. 16, pp. 1963–2010, 2013.

[15] T. G. Ermakova, L. P. Shaulina, N. P. Kuznetsova, L. I. Volkova, A. S. Pozdnyakov, and G. F. Prozorova, "Sorption of noble metal compounds by cross-linked copolymer of 1-vinyl-1,2,4-triazole with acrylic acid," *Russian Journal of Applied Chemistry*, vol. 85, no. 1, pp. 35–40, 2012.

[16] E. Stingaci, M. Zveaghinteva, S. Pogrebnoi et al., "New vinyl-1,2,4-triazole derivatives as antimicrobial agents: synthesis, biological evaluation and molecular docking studies," *Bioorganic & Medicinal Chemistry Letters*, vol. 30, no. 17, Article ID 127368, 2020.

[17] Z. Durmus, B. Unal, M. S. Toprak, A. Aslan, and A. Baykal, "Synthesis and characterization of poly(1-vinyl-1,2,4-triazole) (PVTri)–barium hexaferrite nanocomposite," *Physica B: Condensed Matter*, vol. 406, no. 11, pp. 2298–2302, 2011.

[18] A. S. Pozdnyakov, A. A. Ivanova, A. I. Emel'yanov, Y. I. Bolgova, O. M. Trofimova, and G. F. Prozorova, "Water-soluble stable polymer nanocomposites with AuNPs based on the functional poly(1-vinyl-1,2,4-triazole-co-N-vinylpyrrolidone)," *Journal of Organometallic Chemistry*, vol. 922, Article ID 121352, 2020.

[19] M. Hachemaoui, B. Boukoussa, A. Mokhtar et al., "Dyes adsorption, antifungal and antibacterial properties of metal loaded mesoporous silica: effect of metal and calcination treatment," *Materials Chemistry and Physics*, vol. 256, Article ID 123704, 2020.

[20] M. J. Son and S.-W. Lee, "Antibacterial toxicity of mesoporous silica nanoparticles with functional decoration of specific organic moieties," *Colloids and Surfaces A: Physicochemical and Engineering Aspects*, vol. 630, Article ID 127612, 2021.

[21] S.Ü. Çelik, A. Aslan, and A. Bozkurt, "Phosphoric acid-doped poly(1-vinyl-1,2,4-triazole) as water-free proton conducting polymer electrolytes," *Solid State Ionics*, vol. 179, no. 19-20, pp. 683–688, 2008.

[22] A. Aslan and A. Bozkurt, "Proton conducting properties of ionically cross-linked poly(1-vinyl-1,2,4 triazole) and poly(2-acrylamido-2-methyl-1-propanesulfonic acid) electrolytes," *Polymer Bulletin*, vol. 66, no. 8, pp. 1099–1110, 2011.

[23] A. Aslan, S.Ü. Çelik, Ü. Şen, R. Haser, and A. Bozkurt, "Intrinsically proton-conducting poly(1-vinyl-1,2,4-triazole)/triflic acid blends," *Electrochimica Acta*, vol. 54, no. 11, pp. 2957–2961, 2009.

[24] R. S. Sikorski and P. Hieter, "A system of shuttle vectors and yeast host strains designed for efficient manipulation of DNA in *Saccharomyces cerevisiae*," *Genetics*, vol. 122, no. 1, pp. 19–27, 1989.

[25] H. B. Konuk and B. Ergüden, "Antifungal activity of various essential oils against *Saccharomyces cerevisiae* depends on disruption of cell membrane integrity," *Biocell*, vol. 41, no. 1, pp. 13–18, 2017.

[26] B. Ergüden, "Phenol group of terpenoids is crucial for antibacterial activity upon ion leakage," *Letters in Applied Microbiology*, vol. 73, no. 4, pp. 438–445, 2021.

[27] N. S. Değirmenci, M. Uslu, O. K. Kırbaş, F. Şahin, and E. Önay Uçar, "Lapatinib loaded exosomes as a drug delivery system in breast cancer," *Journal of Drug Delivery Science and Technology*, vol. 75, Article ID 103584, 2022.

[28] C. Gong, L. Yang, J. Zhou, X. Guo, and Z. Zhuang, "Possible role of PAPR-1 in protecting human HaCaT cells against

cytotoxicity of SiO_2 nanoparticles," *Toxicology Letters*, vol. 280, pp. 213–221, 2017.

[29] A. Aslan, Ü. Şen, and A. Bozkurt, "Preparation, properties, and characterization of polymer electrolyte membranes based on poly(1-vinyl-1,2,4 triazole) and poly(styrene sulfonic acid)," *Journal of The Electrochemical Society*, vol. 156, no. 10, Article ID B1112, 2009.

[30] H. Kavas, Z. Durmus, A. Baykal, A. Aslan, A. Bozkurt, and M. S. Toprak, "Synthesis and conductivity evaluation of PVTri–Fe_3O_4 nanocomposite," *Journal of Non-Crystalline Solids*, vol. 356, no. 9-10, pp. 484–489, 2010.

[31] A. Aslan and A. Bozkurt, "Development and characterization of polymer electrolyte membranes based on ionical cross-linked poly(1-vinyl-1,2,4 triazole) and poly(vinylphosphonic acid)," *Journal of Power Sources*, vol. 191, no. 2, pp. 442–447, 2009.

[32] D. Sinirlioglu, A. E. Muftuoglu, and A. Bozkurt, "5-(Methacrylamido)tetrazole and vinyl triazole based copolymers as novel anhydrous proton conducting membranes," *Journal of Polymer Research*, vol. 20, no. 9, 2013.

[33] O. Gómez-Laserna, P. Irizar, G. Lando et al., "Design of epoxy-silica hybrids based on cycloaliphatic diol of natural origin for conservation of lithic materials," *Progress in Organic Coatings*, vol. 151, Article ID 106028, 2021.

[34] Y. Xu, D. Gao, Q. Dong et al., "Anticorrosive behavior of epoxy coating modified with hydrophobic nano-silica on phosphatized carbon steel," *Progress in Organic Coatings*, vol. 151, Article ID 106051, 2021.

[35] A. F. Deyrieux and V. G. Wilson, "In vitro culture conditions to study keratinocyte differentiation using the HaCaT cell line," *Cytotechnology*, vol. 54, no. 2, pp. 77–83, 2007.